JOURNAL OF SOLID STATE CHEMISTRY 64, 249–260 (1986)

New Materials Synthesis: Characterization of Some Metal-Doped Antimony Oxides

RAYMOND G. TELLER,* MARK R. ANTONIO, JAMES F. BRAZDIL, AND ROBERT K. GRASSELLI

Standard Oil Research Center, 4440 Warrensville Center Road, Cleveland, Ohio 44128

Received November 24, 1985; in revised form March 5, 1986

In order to understand the chemistry of altermetal dopants in antimony oxide, the detailed structural characterization of two β-Sb_2O_4 compounds is reported, Mo-doped β-Sb_2O_4 (1.5 metal%) and V-doped β-Sb_2O_4 (5 metal%). The methods used to characterize these materials are X-ray and neutron diffraction, scanning electron microscopy, Mo *K*-edge extended X-ray absorption fine structure spectroscopy, and elemental analysis. The atomic position of each of these dopants in Sb_2O_4 is radically different as is the overall effect on the host structure. Molybdenum does not substitute for Sb atoms, rather the Mo atoms are found in channels of electron density formed by Sb^{3+} lone pairs. The two nearest Sb^{3+} are absent and the oxygen stoichiometry is preserved. The formula is $Sb_{1.97}Mo_{0.015}O_4$. Vanadium incorporates substitutionally for the Sb^{3+} atoms and there are random oxygen vacancies in the resultant structure. The formula is $Sb_{1.9}V_{0.1}O_{3.67}$. In each case the atomic positions of the host structure (Sb and O) are remarkably unaltered. The β-Sb_2O_4 structure can accommodate Mo and V simultaneously, presumably both means of metal incorporation are employed in this ternary oxide.

Introduction

The search for new materials can take several different forms. In classical transition metal or organometallic chemistry, this usually involves the synthesis of new compounds. In solid state chemistry, this can be accomplished by modification of known solids, an example being the investigation of solubilities of metalloids in host oxide frameworks. The dissolution of an element, even in small amounts, into a metal oxide can have a profound effect upon the properties of the host phase. Phase transitions can be triggered at lower temperatures (*1*), and both electronic (*2*) and transport (*3*) properties can be altered. In many cases the alteration of these physical properties can be traced to defect formation in the solid. The catalytic properties, which result from electronic, structural, and defect properties are also affected. The new properties of the doped material are determined by the host lattice in addition to the size, electronic state, and site preference of the dopant. The criteria most often recognized by the solid state chemist in predicting solid solution behavior are size and charge. If a proposed dopant has charge and size that are similar to those of the host lattice atoms, then solid solutions are thought to be attainable. Frequently this is not the case.

* To whom correspondence should be addressed.

0022-4596/86 $3.00

For example, if size and charge were the only important considerations then one would predict that significant amounts of Mo^{5+} (r = 0.63 Å) (*4*) could be substituted for Sb^{5+} (r = 0.61 Å) (*4*) in various oxides of antimony. This has not been found to be true.

The serendipitous discovery that the presence of Mo triggers the α-β transformation of Sb_2O_4 ca. 300°C below the normally observed temperature (1135°C) (*5*) prompted an investigation of the solubilities of certain metals in the antimony oxide structure. While the phase diagram of antimony and oxygen has been thoroughly investigated, the solubilities of other metals in various antimony oxides are virtually unknown. Given that high-temperature phases of antimony oxide (Sb_2O_4) contain both Sb^{3+} and Sb^{5+}, potentially allowing multiple substitution sites, and the importance of Sb_2O_4 phases in catalysis, it was thought that an increased awareness of the factors that govern solid state solubilities in Sb_2O_4 would lead to new materials synthesis. In the course of this work, a report documenting 5% solubility of V in β-Sb_2O_4 appeared in the literature (*6*); this material was subsequently included in our structural study.

Experimental

Materials and methods. Sources of Sb for sample preparation are: stabilized "Sb_2O_5" sol from Nalco or ultrapure Sb_2O_4 or Sb_2O_3 (Alfa Products). Sources for Mo and V are: reagent grade oxides or ammonium salts (molybdate or vanadate). Preparation of samples consisted of either coprecipitating the Sb sol with a solution of ammonium molybdate, followed by gradual evaporation and denitrification or grinding the oxides together prior to firing. In the work presented here, no differences between materials prepared by the two methods were discernable. The final firing temperature for each sample was 850°C.

Neutron diffraction measurements. Time-of-flight neutron diffraction data for three samples were collected: Mo-doped (1.5%) Sb_2O_4, V-doped (5%) Sb_2O_4, and an Sb_2O_4 sample with a larger amount of V. The latter material contains a second phase, $VSbO_4$, in significant amounts. The data were collected at ambient temperature and pressure at Argonne National Laboratory with the IPNS (intense pulsed neutron source) on the special environment powder diffractometer or the general purpose powder diffractometer. Data from the backscattering detectors (2θ = 150°) were used in the refinements, as this is the highest resolution data available from each instrument. The sample was contained within a $\frac{1}{2}$-in.-diameter seamless vanadium tube, capped at both ends with aluminum plugs. Details of the instrument and the data collection and data analysis software package have been previously published (*7*). The raw data has been deposited with the national auxiliary publication service (NAPS).[1] Analysis of the data was performed with a Rietveld profile least-squares program adapted for time-of-flight neutron data and multiphase samples. Starting parameters for the least-squares process were taken from a single crystal study of β-Sb_2O_4 (*8*). In the final least-squares cycles, all parameters for all phases were allowed to vary. The Sb atoms were constrained to lie on symmetry elements as in the X-ray model. The iso-

[1] See NAPS document No. 04393 for 23 pages of supplementary material. Order from ASIS/NAPS. Microfiche Publications, P.O. Box 3513, Grand Central Station, New York, NY 10163. Remit in advance $4.00 for microfiche or $8.65 for photocopy. All orders must be prepaid. Institutions and organizations may order by purchase order. However, there is a billing and handling charge for this service of $15.00. Foreign orders add $4.50 for postage and handling, for the first 20 pages, and $1.00 for additional 10 pages of material. Remit $1.50 for postage of any microfiche orders.

TABLE I

FINAL ATOMIC PARAMETERS FOR β-Sb_2O_4[a]

	Atom	10^4x	10^4y	10^4z	Occupancy[b]
V-doped	Sb(O)	7500	2500	5000	0.500(7)
Sb_2O_4, ave.	Sb(T)	5000	2852(5)	7500	0.467(7)
from two analyses	V(T)	5000	3170(15)	7500	0.042(6)
	O(1)	6916(1)	518(4)	1759(3)	0.93(1)
	O(2)	4064(1)	5878(4)	5349(3)	0.94(1)
Final stoichiometry: $Sb_{1.93}O_{3.71}$ (V content 5 metal%)					
From Mo-doped Sb_2O_4	Sb(O)	7500	2500	5000	0.483(8)
	Sb(T)	5000	2838	7500	0.500(10)
	O(1)	6918(2)	523(4)	1744(4)	1.01(1)
	O(2)	4065(2)	5877(4)	5347(3)	0.99(1)
Final stoichiometry: $Sb_{1.97}O_{4.00}$ (Mo content 1.5 metal%)					
V_2O_5	V[c]	1487	1086	0	$\frac{1}{2}$
	O(1)	1468(4)	4666(13)	320(49)	1
	O(2)	1813(3)	−56(20)	5069(74)	1
	O(3)	0	−30(40)	20(90)	$\frac{1}{2}$
Final stoichiometry assumed to be V_2O_5					

[a] Parameters in this table were taken from the powder neutron profile analysis, except for the position of the V atom in Sb_2O_4, which was taken from an X-ray powder profile analysis.

[b] Occupancies are normalized to complete (crystallographic) occupation of one Sb site.

[c] Values for V were taken from a single crystal X-ray analysis (*10*).

tropic temperature factors of like atoms were constrained to be identical. The occupancy factors of the antimony atoms and oxygen atoms were also varied in separate refinements. Results of these least-squares refinements are reported in Tables I, II, and III. During the analysis of the V-doped Sb_2O_4 samples, a second phase, vanadium antimonate, was included in the refinements. Others have shown that vanadium antimonate is formed when V-doped Sb_2O_4 is held at elevated temperatures (*6*) (>750°C). Vanadium antimonate is a rutile structure, space group $P4_2/mnm$, with the metal atoms randomly occupying a special position (0,0,0). The only refinable structure parameter is the x coordinate of the oxygen atom located at (x,x,0). For these two samples, Sb/V = 19 and Sb/V < 19, the values for x are 0.2958 and 0.3023, respectively. In addition to vanadium antimonate, another phase was evident in the difference pattern in each of these two samples. These were subsequently identified as Al in the Sb/V = 19 sample (from the end caps of the sample holder) and V_2O_5 in the Sb/V < 19 sample. These phases were included in the refinement, and all converged to the values reported in Tables I, II, and III.

Because V has a very small cross section for coherent neutron scattering, its atomic position cannot be directly determined by this method. For this reason, X-ray diffraction data were also collected on the sample of V-doped Sb_2O_4.

Figure 1 displays the diffraction data, calculated plots, and difference plots for the three samples. Scattering lengths used in the refinement are 0.695, 0.564, and 0.580 × 10^{-12} cm for Mo, Sb, and O, respectively.

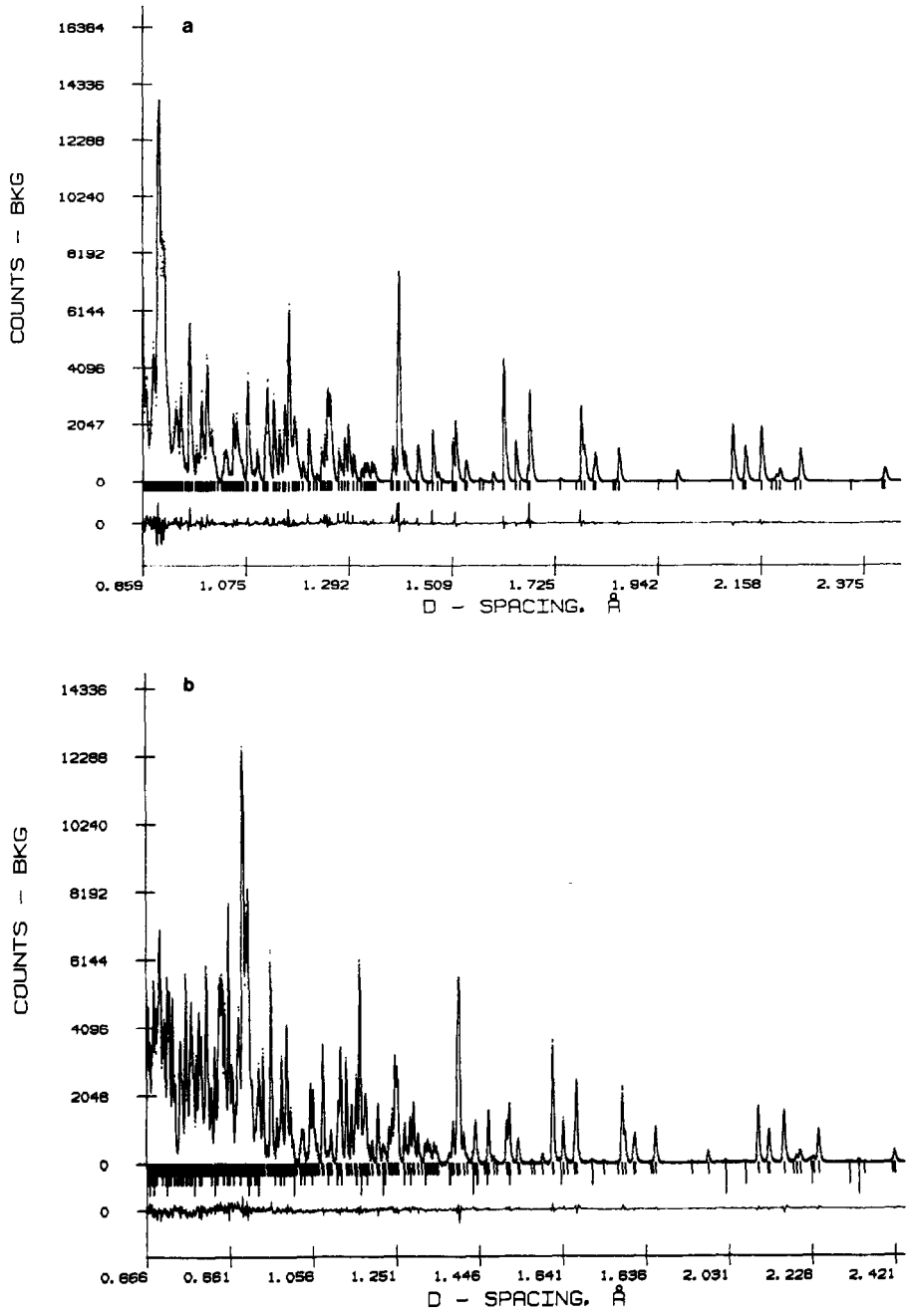

FIG. 1. Powder neutron diffraction data for three samples. Background subtracted data is indicated by points, the calculated diffractogram by a line. A difference curve is presented at the bottom. Tick marks indicate the locations of Bragg reflections. (a) Mo-Doped Sb_2O_4; (b) V-doped Sb_2O_4, Sb/V = 19, short tick marks are for V-doped Sb_2O_4, longer marks for vanadium antimonate, longest marks for aluminum; (c) Sb/V < 19, (= 5), short tick marks are for V-doped Sb_2O_4, longer marks for vanadium antimonate, longest marks for V_2O_5.

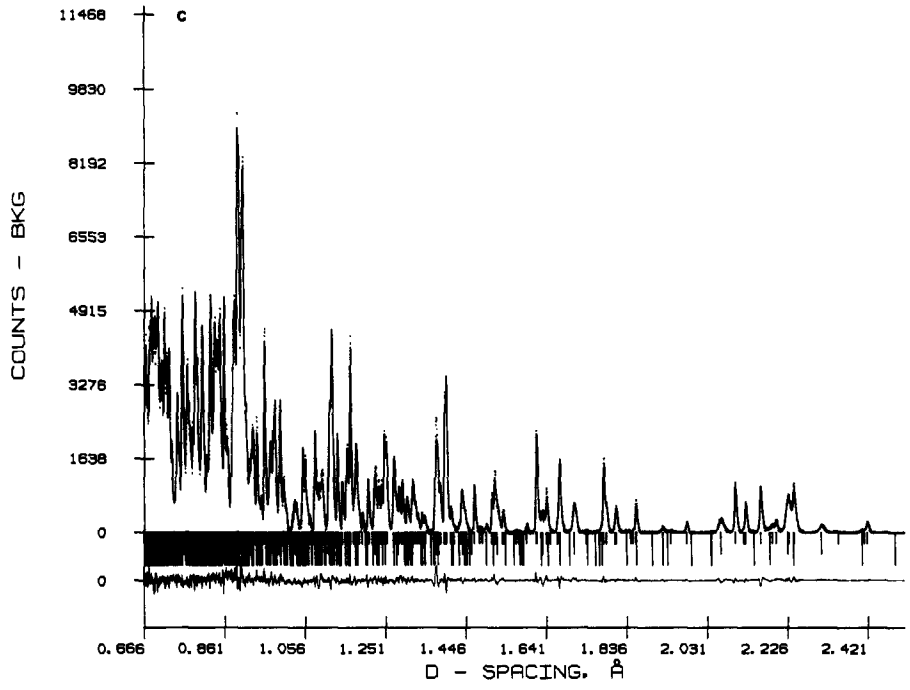

FIG. 1—*Continued.*

X-Ray diffraction measurements. X-Ray diffraction data were collected on a sample of V-doped Sb_2O_4 on a Scintag PAD V automated diffractometer in the step scan mode (0.02° step size, 10 sec count time). The data were fitted with a locally modified ver-

TABLE II

UNIT CELL DIMENSIONS FOR VANADIUM ANTIMONATE STRUCTURES

a, Å	c, Å	V, Å^3	
4.6321(2)	3.0355(2)	65.12(1)	Sb/V = 19, vanadium antimonate epitaxially growth from β-Sb_2O_4 crystallites, $x = 0.2958$
4.6218(1)	3.0476(1)	65.10(1)	Sb/V < 19, excess $V_{1-\alpha}Sb_{1-\alpha}O_4$, $x = 0.3023$
4.624	3.037	64.9	Literature value (11a) of "pure" vanadium antimonate $V_{1-\alpha}Sb_{1-\alpha}O_4$, prepared by firing in air ($\alpha = .08$)
4.608	3.084	65.5	Literature value (11a) of $V_{1.05}Sb_{0.95}O_4$, monoclinic, $b = a$, angle = 90.2

Unit cell dimensions for β-antimony oxide, $C2/c$

a, Å	b, Å	c, Å	β, deg.	V, Å^3	
12.058(3)	4.8316(1)	5.385(1)	104.55(1)	303.7(1)	Sb/V = 19, 5% V
12.057(3)	4.8304(1)	5.388(1)	104.52(1)	303.8(1)	Sb/V < 19, 5% V
12.057(1)	4.8335(1)	5.3838(6)	104.58(1)	303.7(1)	Mo-Doped 1.5%

TABLE III

FINAL REFINEMENT PARAMETERS FOR NEUTRON DATA

A. V-Doped (5%) β-Sb_2O_4, Sb/V = 19, trace $V_{1-\alpha}Sb_{1-\alpha}O_4$		
Time of flight min (*d*-spacing)	7,000 μsec (0.67 Å)	
Time of flight max (*d*-spacing)	26,000 μsec (2.47 Å)	
Half-width parameters (Sb_2O_4)	sig0	1.9
	sig1	7.5
Agreement factors	R_p	2.84%
(No. points on profile = 3801)	R_{wp}	4.08%
(No. variables = 28)	R_{exp}	2.28%
	R_{nucl}	2.93%
Instrument	GPPD	
B. V-Doped (5%) β-Sb_2O_4, Sb/V < 19		
Time of flight min (*d*-spacing)	7,000 μsec (0.67 Å)	
Time of flight max (*d*-spacing)	26,000 μsec (2.47 Å)	
Half-width parameters (Sb_2O_4)	sig0	1.2
	sig1	8.9
Agreement factors	R_p	3.18%
(No. points on profile = 3801)	R_{wp}	4.82%
(No. variables = 41)	R_{exp}	2.37%
	R_{nucl}	3.09%
Instrument	GPPD	
C. Mo-Doped β-Sb_2O_4, Sb/Mo = 130		
Time of flight min (*d*-spacing)	6,500 sec (0.85 Å)	
Time of flight max (*d*-spacing)	20,000 μsec (2.42 Å)	
Half-width parameters (Sb_2O_4)	sig0	4.2
	sig1	9.5
Agreement factors	R_p	4.4%
(No. points on profile = 2701)	R_{wp}	5.9%
(No. variables = 25)	R_{exp}	2.7%
	R_{nucl}	3.5%
Instrument	SEPD	

Note. The peak shape profile function *P*(delt) takes the following form: *P*(delt) = [0.5 * ALP * BET/(ALP + BET)] * [EXP(*U*) * ERFC(*Y*) + EXP(*V*) * ERFC(*Z*)]; where: delt = *d*-spacing (TOF) -- *d*-spacing (Bragg refl.) sig1 and sig0 are involved in calculating *U*, *Y*, *V*, and *Z*; and other quantities are fixed parameters determined by fitting a standard.

sion of DBW 3.2 (*9*). A pseudo-Voight function was used to fit the peak profile. Other parameters varied included a three-parameter background function, a scale factor for each phase, cell and asymmetry parameters, preferred orientation, two theta zero, and profile parameters. Positional and occupancy values for the Sb and O atoms were fixed at values taken from the neutron refinement. Thermal parameters for all atoms were allowed to vary, as were the positional and occupancy parameters for the V atom position.

X-Ray absorption measurements. Molybdenum *K*-edge X-ray absorption data for Mo-doped Sb_2O_4 were obtained at approximately 80 K in the transmission mode at the Stanford Synchrotron Radiation Laboratory (SSRL) on beam line I-5. The mode of collection and analysis procedure have been reported elsewhere (*5*).

Physical measurements. Samples were also examined by scanning electron microscopy (SEM) with a Cambridge Instruments Camscan, equipped with a Kevex energy dispersive X-ray (EDX) analyzer. EDX analysis of a number of well-formed crystals was used to determine Mo content in Mo-doped Sb_2O_4. Examination of all samples revealed that all phases present consisted of large (30 μm) well-formed platelike crystals.

Discussion

We have noted that the presence of Mo lowers the α-to-β transition temperature in Sb_2O_4 to ca. 800°C. Berry *et al.* have noted that V has the same effect (*6*). In each case, β-Sb_2O_4 is the only observed phase (for 5% V doping a trace amount of vanadium antimonate is noted upon prolonged heating), and this implicates solid solubility of each of these elements in the β-Sb_2O_4 structure. This hypothesis is supported by the structural work presented herein, electron microscopy reported here and elsewhere (*6*), as well as the pronounced color change noted upon compound formation (undoped β-Sb_2O_4 is white, V doping introduces a deep brown color, molybdenum doping a tan-orange color). It is also possible for both elements, V and Mo, to be simultaneously incorporated into the antimony oxide framework.

Powder neutron diffraction structure description. The structure of β-Sb_2O_4 has been described previously on the basis of a single crystal X-ray diffraction analysis (*8*). The powder neutron diffraction results described herein corroborate this work, although the inherently greater sensitivity of neutrons to oxygen atom positions results

TABLE IV

DISTANCES (IN Å) AND ANGLES (IN DEGREES) WITHIN THE COMPOUNDS REFINED

β-Sb_2O_4:	Distances	From V-doped Sb_2O_4	From Mo-doped β-Sb_2O_4
	Sb(T)–O(2)	2.024(3) ×2	2.029(2) ×2
	O(2)′	2.208(3) ×2	2.208(2) ×2
	···O(1)	2.937(3) ×2	2.931(2) ×2 (Nonbonding)
	Sb(O)–O(1)	1.963(2) ×2	1.957(2) ×2
	–O(1)′	1.963(2) ×2	1.968(2) ×2
	–O(2)	2.005(2) ×2	2.008(2) ×2
	V(T)–O(2)	1.92(6)	
	–O(2)′	2.17(2)	
	Angles (large and small angles across the square pyramid)		
	α	147.8(1)	147.3(1)
	β	73.3(1)	73.0(1)
	for V : α	155(5)	
	β	76(2)	
$V_{1-\alpha}Sb_{1-\alpha}O_4$:	Distances,	Sb/V = 19	Sb/V < 19
	(2×)*M*–O	1.938(1)	1.976(2)
	(4×)*M*–O	2.023(1)	1.998(2)
Shortest	O···O	2.67	2.58
V_2O_5:	Distances	This work	Literature values
	V–O(1)	1.569(7)	1.586(4)
	–O(3)	1.786(12)	1.745(2)
	–O(2)	1.862(25)	1.865(2)
	–O(2)′	1.909(25)	1.889(2)
	–O(2)″	2.015(12)	2.022(3)
	–O(1)′	2.809(7)	2.788(5)
Shortest	O···O	2.38	2.39

in more precise Sb—O bond lengths and angles. Final positional parameters and selected distances and angles are listed in Table IV. The structure consists of corrugated layers of corner-linked SbO_6 octahedra (5+ ox. state Sb(O)) separated by sheets of SbO_4 polyhedra (3+ ox. state Sb(T)). The Sb(O) atoms lie on a crystallographic inversion center and the octahedron of O atoms are very symmetrically displaced about the metal atom. In contrast to this, the ligating oxygen atoms are very asymmetrically disposed about the Sb(T) atoms. The Sb(T) atoms are constrained to lie on a crystallographic twofold axis. This asymmetry is undoubtedly due to the presence of the Sb(T) lone electron pair. The coordination about these Sb(T) atoms can be envisioned as octahedral with two ligands removed to accommodate the lone pair. The remaining oxide ligands are then bent away from the lone pair, leading to the observed distorted oxygen environment. The [001] face of the structure is displayed in Fig. 2. The Sb(T) lone pairs can be seen as lining up to form channels (crystallographic direction: $\frac{1}{2}$, 0, z) of electron density perpendicular to the [001] face. Because the Sb atoms are located on symmetry elements, the Sb_2O_4 stoichiometry is arrived at by doubling the refined occupancies reported in Table I.

The α-Sb_2O_4 structure is similar to the

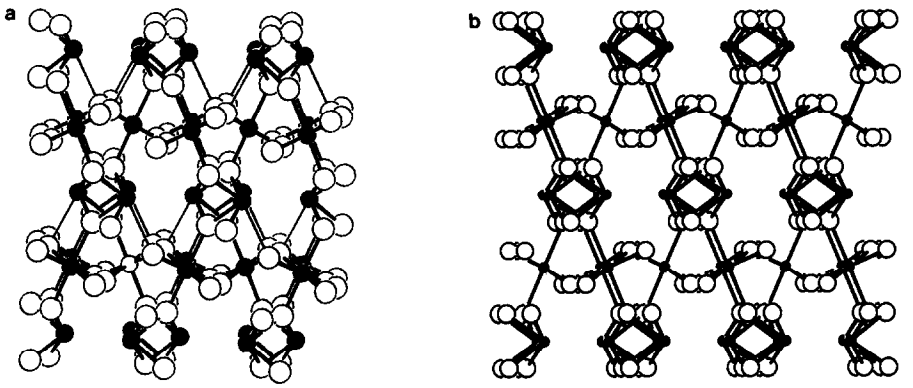

FIG. 2. (a) α-Antimony oxide (α-Sb_2O_4), [100] face. (b) β-antimony oxide (β-Sb_2O_4). Filled spheres represent Sb atoms; open spheres, oxygen atoms. Note the two kinds of coordination for the two types of Sb atoms. Sb^{5+} atoms (identified as Sb(O) in the text) are octahedrally coordinated. The asymmetric coordination of the Sb^{3+} (identified as Sb(T) in the text) is due to the presence of a lone electron pair; these form channels of electron density perpendicular to the views presented here. These Sb atoms are four-coordinate in the β form. In the α form, a fifth oxygen (2.59 Å) is weakly bonded to Sb^{3+}. There are two types of oxygen atoms in β-Sb_2O_4, one type bridges Sb(O) atoms only, while the second type bridges Sb(T) and Sb(O) atoms.

beta structure (Fig. 2), but of a lower symmetry. A major difference between the α and β form is in the coordination of the Sb^{3+} ions. In the β structure four oxygen atoms are within bonding distance, whereas in the α structure a fifth oxygen atom comes within bonding distance (albeit a weak bond) of the Sb(T) atoms.

Location of dopants within the β-Sb_2O_4 structure. A combination of Mo *K*-edge EXAFS and powder neutron diffraction profile analysis has been utilized in determining the atomic position of Mo within β-Sb_2O_4. This work has been described in detail elsewhere (*5*), and only a summary of the findings are presented here. The low level of Mo doping possible (1.5%) precludes the use of diffraction measurements to directly locate the Mo atoms. The diffraction data indicates that the host structure is unperturbed (Table IV), with the exception of ca. 3% vacancy of the Sb(T) atoms. This is consistent with electrical neutrality requirements. Analysis of the EXAFS data indicates that the Mo atom is surrounded by 3–5 nearest oxygen neighbors; the average Mo—O interatomic distance is 1.96 Å. The next nearest neighbor average interatomic distance (Mo—Sb) and coordination number is 3.36 Å and 1–2, respectively. Examination of distances and angles in the β-Sb_2O_4 structure indicates that substitution of Mo for either antimony atoms, Sb(O) or Sb(T), is unlikely. The symmetric octahedral site, while matching the EXAFS determined Mo—O bond distance is six-coordinate, not three- to five-coordinate. Additionally, a "white line" pre-edge feature is observed ($s \rightarrow nd$ transition) in the Mo X-ray absorption near-edge data; this is also inconsistent with substitution of Mo in the Sb(O) site. The asymmetric Sb site, while four-coordinate, would probably serve as a Mo site, but the diffraction experiments indicated a 3% vacancy at Sb(T). There exists an interstitial site within the β-Sb_2O_4 structure, however, that fits both the diffraction and spectroscopic data. At a point along a line ($\frac{1}{2}$,0,z, $z = \frac{1}{2}$) that contains the Sb lone pairs, there is a four-coordinate oxygen site that could accommodate the Mo atom. The two nearest

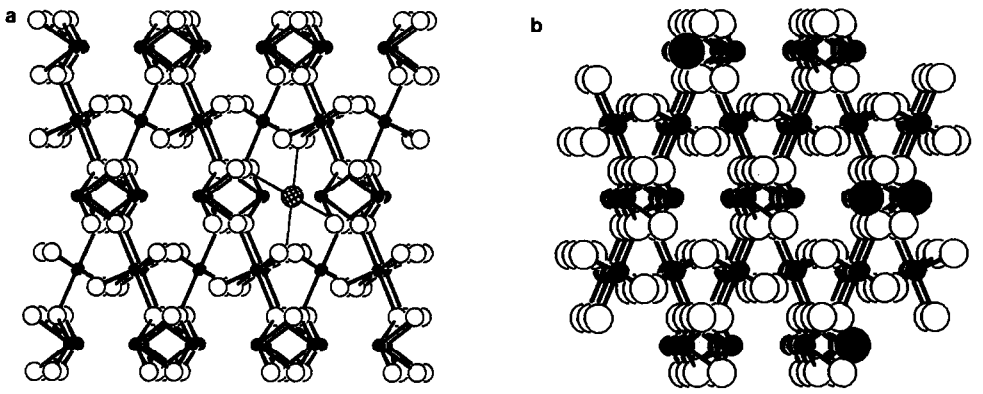

FIG. 3. The structures of doped β-Sb_2O_4, filled spheres represent Sb atoms, open spheres oxygen atoms. (a) Mo is represented as a cross-hatched sphere and is located within channels of electron density. The two Sb^{3+} atoms nearest the Mo atom have been removed. (b) V substitutes for Sb^{3+} atoms and is represented by larger filled spheres.

Sb(T) atoms are too close (ca. 2.0 Å) and are required to be vacant (hence the 3% observed vacancy). The next two nearest Sb atoms are 3.35 Å. It is hypothesized that this is the site of Mo incorporation within β-Sb_2O_4; this is illustrated in Fig. 3a.

Refinements of the powder neutron diffraction data for V-doped β-Sb_2O_4 revealed a different picture. Because V atoms have a very small coherent scattering length for thermal neutrons, their locations cannot be determined directly with neutron data. In a sense, however, the lack of coherent scattering by V presents an ultimate contrast from other elements, and a partial Sb vacancy suggests partial V substitution. Such is the case for V-doped β-Sb_2O_4. As reported in Table I, the stoichiometry of two samples of varying V content (each of which contained at least the maximum reported solubility of V, excess V found in vanadium antimonate) averaged $Sb_{1.93}O_{3.71}$. The oxygen vacancies are randomly dispersed between the two oxygen sites, the Sb vacancy is localized on one site, Sb(T). X-Ray powder diffraction data were collected and analyzed for one of the samples (Sb/V = 19). Least squares analysis of this data converged to a 8.5% occupancy of V at a location 0.15 Å distant from the Sb(T) site. Hence the formula of this material is $Sb_{1.93}V_{0.08}O_{3.73}$, and V substitutes at or near the asymmetric Sb site. Note that the oxygen vacancy of this material requires that some of the Sb(O) atoms be +3 charged. This vanadium substitution is illustrated in Fig. 3b.

V_2O_5 structure. The structure of crystalline V_2O_5 is known (*10*) although there is some controversy over the correct space group. From our refinements, we have found that the correct space group is $Pnm2_1$ (a = 11.555(1), b = 4.371(1), c = 3.557(1) Å). Our structural results (as indicated in Table IV) are in excellent agreement with those in the literature. The coordination geometry about the V atoms is much like a square pyramid. The apical oxygen is quite close to the V atom (V=O), whereas the four equitorial oxygen atoms are normal, i.e., single, M—O distances away. The sixth distant oxygen is trans to the short V=O bond, and is very weakly bound to the V atom. As such this coordination is best described as a pyramidally distorted octahedron. This geometry is reminiscent of that of Sb(T) in Sb_2O_4 with the lone pair at the apex. It is worthwhile to

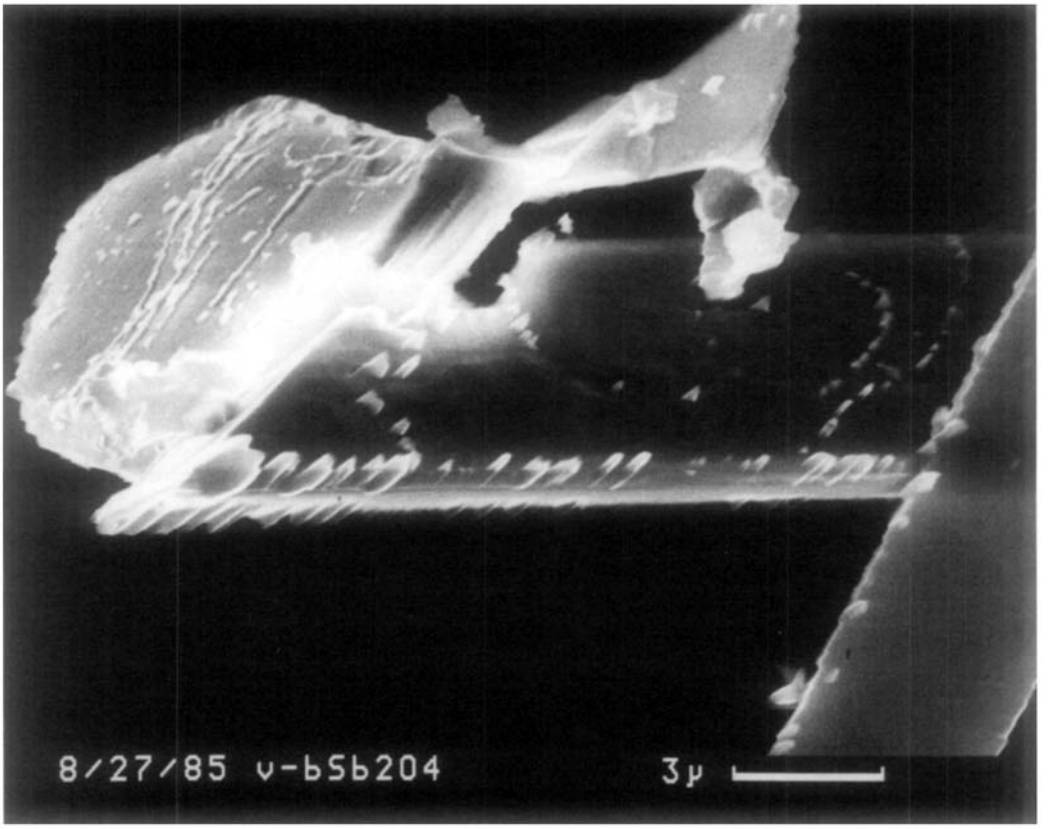

FIG. 4. SEM micrograph of V-doped Sb_2O_4. Note the outgrowths of small crystallites on the large crystals of antimony oxide. These have been identified as vanadium antimonate (Ref. (*6*)).

note that in all known vanadium oxide structures, the V atoms are either found in significantly distorted octahedrons or tetrahedra.

Vanadium antimonate structures. Vanadium antimonate possesses a nonstoichiometric rutile structure; the exact formula of which depends upon the atmosphere during firing (*11*). In air at 800°C, antimony oxide and vanadium oxide react to form $V_{1-x}Sb_{1-x}O_4$ ($0 < x < 0.08$). Antimony Mössbauer experiments identify the Sb oxidation state as 5+; this requires that the V be mixed valent (most likely 3+ and 4+). Under a nitrogen atmosphere $V_{1+x}Sb_{1-x}O_4$ ($0 < x < 0.08$) is formed. These materials have slightly different structures that reflect their chemical differences (*11a*). Stoichiometric $VSbO_4$ (V^{3+}, Sb^{5+}) is not known. Berry *et al.* have noted that prolonged heating of V-doped β-Sb_2O_4 produces small crystallites of vanadium antimonate that apparently grow out of the faces of the β-Sb_2O_4 (*6*). SEM micrographs of this phenomenon are reproduced in Fig. 4. There is an apparent orientation of these crystallites. Lattice matching calculations (*12*) indicate that there are several good (i.e., less than 10^9 dislocations/cm^2) unit cell matches between these crystals ([010] for vanadium antimonate and $[\bar{1}10]$, [001], and $[\bar{1}01]$ for β-Sb_2O_4). A comparison of the atomic arrangements of these faces also indicates that the atoms are well situated for

epitaxial growth. These results suggest that the small vanadium antimonate crystals are epitaxially grown from the faces (or edges) of the vanadium-doped antimony oxide crystals. In order to determine if there is any structural difference between epitaxially grown and "normally" synthesized vanadium antimonate, neutron diffraction data of two samples, Sb/V = 19 (V-doped β-Sb_2O_4/epitaxy $VSbO_x$) and Sb/V < 19 (V-doped β-Sb_2O_4/$VSbO_x$) are compared here.

Examination of Table II reveals a difference in lattice parameters between the two samples containing vanadium antimonate. The *a* and *b* lattice parameters (required to be equal by symmetry) of $V_{1-\alpha}Sb_{1-\alpha}O_4$ as grown epitaxially from antimony oxide are expanded (0.2%) with respect to the other sample containing vanadium antimonate. Conversely, *c* is contracted (this difference (0.2%) is well within the precision of the measurements). Apparently, the difference between these two forms of vanadium antimonate is due to the different mechanisms of crystal growth. The strain produced in epitaxially grown "$VSbO_4$" is further documented by the distance and angle calculations in Table IV. The metal–oxygen octahedron is symmetric for "normal" $V_{1-\alpha}Sb_{1-\alpha}O_4$. For the epitaxially grown $V_{1-\alpha}Sb_{1-\alpha}O_4$ (Sb/V = 19), the octahedron is somewhat squashed. The question arises whether this distortion is confined to the interface between the two types of crystals or if the bulk structure is also distorted. The structure at the interface is expected to be more affected because the atoms at or near the interface must be distorted from their "normal" positions to accommodate the neighboring phase, allowing epitaxial growth. Since diffraction measurements are sensitive to the bulk structure, the answer is apparently that the bulk structure is altered. However, for small crystallites, a significant portion of the atoms are at or near the surface, and a bulk measurement will be heavily weighted by these surface (3–5 layers) atoms. This distortion would not be evident in diffraction experiments on large crystals because the surface accounts for so little of the mass of the crystal. Examination of Fig. 4 reveals that the vanadium antimonate crystals are of the order of 1 μm (10^4 Å). As 3–5 layers (unit cells) takes up only 12–20 Å, it appears that the atoms at or near the interface make up an extremely small percentage of the total, and that the bulk structure of $V_{1-\alpha}Sb_{1-\alpha}O_4$ grown epitaxially from β-Sb_2O_4 is indeed different from that of free $V_{1-\alpha}Sb_{1-\alpha}O_4$ grown without the aid of epitaxy.

The differences between these vanadium antimonate structure "types" could be due to different mechanisms of crystal growth (combination of the oxides vs epitaxial growth) or differences in composition that are a consequence of epitaxial growth. It is unlikely that the epitaxially grown $VSbO_4$ is vanadium rich as the cell parameters of this material differ significantly from those of $V_{1.05}Sb_{0.95}O_4$ (see Table II). That epitaxially grown vanadium antimonate is Sb rich remains a possibility.

Summary

This work serves to document the solubility of Mo (1.5%) and V (5%) in β-Sb_2O_4. Furthermore, the mode of altermetal incorporation has been shown to be markedly different. Mo atoms are found in regions of lone pair electron density with the concurrent absence of the two nearset Sb(T) atoms. Vanadium has been found to substitute for Sb(T) atoms, additionally some random oxygen vacancies are observed. These results are somewhat unexpected. Given the similarity in atomic radii of Sb^{5+}, V^{3+}, and Mo^{6+}, one might have expected the Mo or V atoms to substitute for Sb(O) atoms, but this is not the case. This is undoubtedly due to coordination environment preferences. When in an octahedral oxygen environment, both Mo and V are observed

to prefer distorted environments (*13*) and both metals are known to display tetrahedral oxygen coordination in numerous oxides. These examples strengthen the notion that the electronic state of a potential dopant (operationally referred to here as coordination environment preference) are at least as important in determining modes of substitution in oxide structures as is size.

The ability of nonstoichiometric vanadium antimonate to accommodate differing amounts of metal, depending upon sintering environment, is known (*11*). Results of neutron diffraction analysis also reveal that the vanadium antimonate structure can also adjust depending upon the mode of synthesis. When grown epitaxially from β-Sb_2O_4, the unit cell and atom positions within the cell indicate that the solid is expanded along two directions, and contracted along the third (*c*-axis) direction as compared to conventionally synthesized material. While it is known that a particular polymorph or polytype can be preferentially grown by epitaxy, it has never before been demonstrated that the bulk structure of a compound could be affected utilizing an epitaxial growth mechanism.

Acknowledgments

The authors gratefully acknowledge fruitful discussions with Professor E. Kostiner (University of Connecticut), Dr. G. Shoemaker and E. Armstrong (Standard Oil Research Center). The authors acknowledge the U.S. Department of Energy for supporting the Intense Pulsed Neutron Source at Argonne National Laboratory as a national user's facility and the Standard Oil Company for permission to publish this work.

Note added in proof: V K-edge X-ray absorption measurements of vanadium-doped Sb_2O_4 have served to identify the oxidation state of the V atoms as +5 and the vanadium–oxygen coordination environment as asymmetric. Raman data indicate the presence of vanadyl groups $(V{=}O)^{+3}$ within this structure as well.

References

1. J. Stocker, *Bull. Soc. Chim., Fr.*, 78 (1961).
2. A. Hooper, *J. Phys. D. Appl. Phys.* **10,** 1487 (1977).
3. T. H. Etshell and S. N. Flengas, *Chem. Rev.*, 339 (1970).
4. J. E. Huheey, "Inorganic Chemistry," p. 75, Harper & Row, New York (1975).
5. R. G. Teller, M. R. Antonio, J. F. Brazdil, R. K. Grasselli, and M. Mehicic, *Inorg. Chem.* **24,** 3370 (1985).
6. F. J. Berry, M. E. Brett, and W. R. Patterson, *J. Chem. Soc., Dalton Trans.*, 13 (1983).
7. (a) J. R. Hauman, R. T. Daley, T. G. Worlton, and R. K. Crawford, *IEEE Trans. Nucl. Sci.* **NS-29,** 62 (1982); (b) R. B. Von Dreele, J. D. Jorgensen, and C. G. Windsor, *J. Appl. Crystallogr.* **15,** 581 (1982); (c) J. D. Jorgensen and J. Faber, "ICANS-II, Proc. VIth Int. Collab. Adv. Neutron Sources," Argonne Natl. Lab., June 28–July 2, 1982 (ANL-82-80, 1983).
8. (a) A. C. Skapski and D. Rogers, *J. Chem. Soc. Chem. Commun.*, 611 (1965); (b) D. Rogers and A. C. Skapski, *Proc. Chem. Soc.*, 400 (1964).
9. D. B. Wiles and R. A. Young, *J. Appl. Crystallogr.* **14,** 149 (1981).
10. H. G. Bachmann, F. R. Ahmed, and W. H. Barnes, *Z. Kristallogr.* **115,** 110 (1961).
11. (a) T. Birchall and A. W. Sleight, *Inorg. Chem.*, 868 (1976); (b) F. J. Berry and M. E. Brett, *J. Chem. Soc., Dalton Trans.*, 9 (1983).
12. B. Dickens and L. W. Schroeder, *J. Res. Nat. Bur. Stand.* **85,** 347 (1980).
13. A. F. Wells, "Structural Inorganic Chemistry," 5th ed., pp. 572, 565, 566, Oxford Univ. Press (Clarendon), London/New York (1975).